

# *Propagation and transformation of upper North Atlantic deep water from the subpolar gyre to 26.5°N*

Article

Accepted Version

Creative Commons: Attribution 4.0 (CC-BY)

Open Access

Petit, T. ORCID logo ORCID: <https://orcid.org/0000-0002-7922-9363>, Lozier, M. S., Rühls, S. ORCID logo ORCID: <https://orcid.org/0000-0001-5001-4994>, Handmann, P. ORCID logo ORCID: <https://orcid.org/0000-0002-5901-4680> and Biastoch, A. ORCID logo ORCID: <https://orcid.org/0000-0003-3946-4390> (2023) Propagation and transformation of upper North Atlantic deep water from the subpolar gyre to 26.5°N. *Journal of Geophysical Research: Oceans*, 128 (8). e2023JC019726. ISSN 2169-9291 doi: <https://doi.org/10.1029/2023jc019726> Available at <https://centaur.reading.ac.uk/113052/>

It is advisable to refer to the publisher's version if you intend to cite from the work. See [Guidance on citing](#).

To link to this article DOI: <http://dx.doi.org/10.1029/2023jc019726>

Publisher: American Geophysical Union (AGU)

All outputs in CentAUR are protected by Intellectual Property Rights law, including copyright law. Copyright and IPR is retained by the creators or other copyright holders. Terms and conditions for use of this material are defined in

the [End User Agreement](#).

[www.reading.ac.uk/centaur](http://www.reading.ac.uk/centaur)

## **CentAUR**

Central Archive at the University of Reading

Reading's research outputs online

1 **Propagation and Transformation of upper North Atlantic Deep Water from the subpolar**  
2 **gyre to 26.5°N**

3 T. Petit<sup>1,a</sup>, M.S. Lozier<sup>1</sup>, S. Rühs<sup>2,b</sup>, P. Handmann<sup>2</sup>, A. Biastoch<sup>2,3</sup>

4 <sup>1</sup> School of Earth and Atmospheric Sciences, Georgia Institute of Technology, Atlanta, GA, USA

5 <sup>2</sup> GEOMAR Helmholtz Centre for Ocean Research Kiel, Kiel, Germany

6 <sup>3</sup> Kiel University, Kiel, Germany

7 <sup>a</sup> Present address: National Centre for Atmospheric Science, Department of Meteorology, University of Reading,  
8 Reading, UK

9 <sup>b</sup> Present address: Institute for Marine and Atmospheric research Utrecht, Utrecht University, Netherlands

10

11 **Key points**

- 12 • The large majority of uNADW sourced from the Irminger Sea transits through the  
13 Labrador Sea before reaching 26.5°N
- 14 • Interior pathways along the eastern flank of the Mid-Atlantic Ridge connect the Iceland  
15 Basin and Rockall Trough to 26.5°N
- 16 • Though uNADW is mainly sourced in the eastern subpolar gyre, its transit in the  
17 Labrador Sea is associated with further property changes

18 **Abstract**

19 Because new observations have revealed that the Labrador Sea is not the primary source for waters  
20 in the lower limb of the Atlantic Meridional Overturning Circulation (AMOC) during the OSNAP  
21 period, it seems timely to re-examine the traditional interpretation of pathways and property  
22 variability for the AMOC lower limb from the subpolar gyre to 26.5°N. In order to better  
23 understand these connections, Lagrangian experiments were conducted within an eddy-rich ocean  
24 model to track upper North Atlantic Deep Water (uNADW), defined by density, between the  
25 OSNAP line and 26.5°N as well as within the Labrador Sea. The experiments reveal that 77% of  
26 uNADW at 26.5°N is directly advected from the OSNAP West section along the boundary current  
27 and interior pathways west of the Mid-Atlantic Ridge. More precisely, the Labrador Sea is a main  
28 gateway for uNADW sourced from the Irminger Sea, while particles connecting OSNAP East to  
29 26.5°N are exclusively advected from the Iceland Basin and Rockall Trough along the eastern  
30 flank of the Mid-Atlantic Ridge. Although the pathways between OSNAP West and 26.5°N are  
31 only associated with a net formation of 1.1 Sv into the uNADW layer, they show large density  
32 changes within the layer. Similarly, as the particles transit through the Labrador Sea, they undergo  
33 substantial freshening and cooling that contributes to further densification within the uNADW  
34 layer.

## 35 **Plain Language Summary**

36 The North Atlantic Deep Water (NADW) is a cold and fresh water mass formed at high latitudes  
37 and advected southward across the North Atlantic as part of the Atlantic Meridional Overturning  
38 Circulation (AMOC). The upper part of this water mass (uNADW) has long been considered to be  
39 mainly formed in the Labrador Sea. However, new observations have revealed that the Labrador  
40 Sea is not the primary source for uNADW, suggesting that the dense water observed at 26.5°N is  
41 not necessarily related to Labrador Sea convection. Here, we perform Lagrangian experiments  
42 between the subpolar gyre and 26.5°N within an eddy-rich ocean model to show that the Labrador  
43 Sea is a main gateway for uNADW sourced from the Irminger Sea and is associated with large  
44 property changes within the uNADW layer. Additionally, we reveal direct interior pathways  
45 connecting uNADW sourced from the Iceland Basin and Rockall Trough to 26.5°N.

## 46 **1. Introduction**

47 For decades, the Labrador Sea was thought to be the primary source of deep water formed in the  
48 subpolar North Atlantic (McCartney & Talley, 1982; Pickart et al., 2003; Rhein et al., 2002;  
49 Straneo et al., 2003; Yashayaev et al., 2007) and carried equatorward via the deep limb of the  
50 Atlantic Meridional Overturning Circulation (AMOC). However, observations from the  
51 Overturning in the Subpolar North Atlantic Programme (OSNAP) have revealed that dense water  
52 formed between the Greenland Scotland Ridge (GSR) and OSNAP East, the latter of which spans  
53 a section from the Scottish shelf to the southeast tip of Greenland, contributes far more to the  
54 AMOC lower limb than that formed in the Labrador Sea (Lozier et al., 2019).

55 More precisely, the Irminger and Iceland basins are one of the main sources of dense water formed  
56 in the subpolar North Atlantic (Chafik & Rossby, 2019; Petit et al., 2020; Tooth et al., 2022).  
57 There, warm and salty water from the subtropical gyre is transformed into cold dense water largely  
58 via wintertime convection. Thus, the OSNAP results suggest that the dominant sources for the  
59 AMOC lower limb are overflow water transported from the Nordic Seas through the GSR and  
60 upper North Atlantic Deep Water (uNADW) formed in the Irminger and Iceland basins. The net  
61 formation of deep water through wintertime convection in the Labrador Sea, estimated as the  
62 maximum of the overturning stream functions, is seven times smaller than in the eastern subpolar  
63 gyre and thus contributes minimally to the mean overturning strength during the OSNAP period  
64 (Li et al., 2021b). The interannual variability of the AMOC is also dominated by the eastern

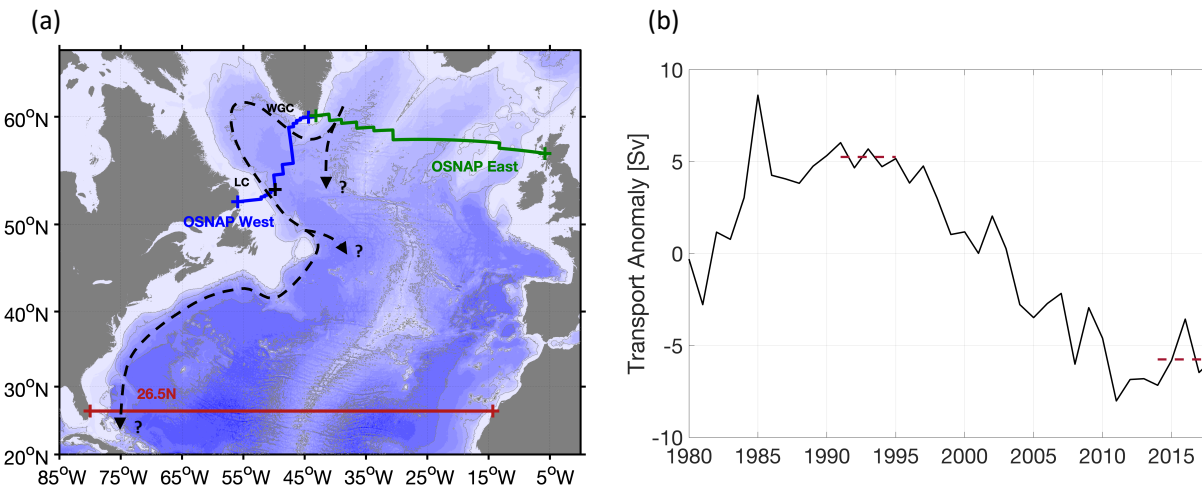
65 subpolar gyre, such that ventilation in the Labrador Sea is unlikely to play a leading role in the  
66 connectivity mechanism between the subpolar and subtropical gyres identified by Kostov et al.  
67 (2022) on fast interannual timescales. However, Yeager et al. (2021) uses a long CESM integration  
68 to show that deep water formation in the western subpolar gyre dominates the AMOC variability  
69 at low frequencies. Two other reasons to highlight the contribution of the Labrador Sea come from  
70 recent studies: Freshwater fluxes across OSNAP West are a strong contributor to the total  
71 meridional freshwater flux across the entire OSNAP section (Li et al., 2021a) and ventilation of  
72 dense water in the Labrador Sea is important for the uptake, storage and export of oxygen in the  
73 AMOC lower limb (Koelling et al., 2022).

74 Because deep water formed in the Labrador Sea was long considered the main source of water for  
75 the AMOC lower limb, downstream analyses of AMOC variability have generally been interpreted  
76 in terms of Labrador Sea Water (LSW) variability, particularly so at 26.5°N (Frajka-Williams et  
77 al. (2016) and Jackson et al. (2016)). Previous studies have interpreted the lag between LSW  
78 production and its arrival at 26.5°N as the advective time scale for LSW anomalies to exit the  
79 Labrador basin and travel along the Deep Western Boundary Current (DWBC) and interior  
80 pathways (Biló & Johns, 2019; Bower et al., 2009). For instance, Van Sebille et al. (2011) and  
81 Molinari et al. (1998) estimated a lag of 9-10 years for the LSW salinity anomaly in the Labrador  
82 Sea to reach 26.5°N. Curry et al. (1998), who also linked the variability of subtropical temperature  
83 at intermediate depths near Bermuda to the variability of convection in the Labrador Sea, yet found  
84 a lag of only 6 years. More recently, Chomiak et al. (2022) found longer advection timescales of  
85 10-15 years from a study of both salinity and temperature anomalies of the LSW layer.  
86 Importantly, all of these studies implicitly assume that all waters that reach 26.5°N in the LSW  
87 density range are primarily sourced by Labrador Sea convection, as opposed to the eastern subpolar  
88 North Atlantic. However, given our new understanding of the sources of dense water for the  
89 AMOC during the OSNAP period, it seems timely to re-examine the traditional interpretation of  
90 pathways and property variability for the AMOC lower limb from the subpolar gyre to 26.5°N.

91 We posit that there are two possibilities for the pathways of uNADW sourced in the eastern  
92 subpolar gyre: 1) the uNADW is mainly advected southward from OSNAP East through various  
93 interior pathways, as recently shown for the overflow water (Lozier et al., 2022; Zou et al., 2020b)  
94 or 2) a majority of uNADW flows into and out of the Labrador Sea before being exported  
95 southward to 26.5°N, along the DWBC and interior pathways.

96 To connect downstream property variability with source water variability, we aim to assess  
 97 whether uNADW sourced in the eastern subpolar gyre is further transformed within the uNADW  
 98 layer once it crosses OSNAP East. Thus, in addition to understanding the pathways of these dense  
 99 waters we will examine the degree to which the uNADW layer is modified as it moves equatorward  
 100 and, in particular, as it moves through the Labrador Sea.

101 In summary, we aim to investigate the mean pathways and along-track property transformation of  
 102 uNADW between OSNAP East and 26.5°N (Figure 1a) to better connect downstream and  
 103 upstream deep-water properties. We introduce our Lagrangian experiments in section 2, discuss  
 104 the experimental results in section 3, investigate uNADW transformation over the Labrador Sea  
 105 in section 4 and then summarize our results in section 5.



106 **Figure 1.** (a) Definition of the sections OSNAP East, OSNAP West and 26.5°N used in the set of experiments  
 107 EXP\_1 in VIKING20X-JRA-short. The sections LC and WGC used for the set of experiments EXP\_2 follow  
 108 the OSNAP West section and are separated by the black cross. The black arrows indicate two possible pathways  
 109 for uNADW: through the interior or along the boundary via the Labrador Sea. (b) Transport anomaly (Sv) for  
 110 the uNADW layer as compared to the 1980-2018 mean at the LC section. Dashed red lines indicate the averaged  
 111 uNADW transport in 1991-1995 and 2014-2018. Positive transports are southward and hence represent export  
 112 out of the Labrador Sea.  
 113

## 114 2. Data and Methods

### 115 2.1 Observational data from OSNAP and WOCE

116 Two sets of observations are used to compare the volume transports for the AMOC lower limb  
 117 between the subpolar gyre and 26.5°N. At subpolar latitudes, we use the monthly estimates of

118 transports across the OSNAP (Overturning in the Subpolar North Atlantic Program) array from  
119 April 2014 to August 2018 (Li et al., 2021b). The gridded ( $\sim 25 \times 20$  km) cross-section transports  
120 are estimated from continuous measurements of salinity, temperature and velocity following the  
121 International Thermodynamic Equation of Seawater-2010 (TEOS-10, Li et al., 2017). The  
122 transport in the AMOC lower limb, defined as water denser than  $\sigma_2 = 36.5 \text{ kg m}^{-3}$  in Van Sebille  
123 et al. (2011), ranges from 15.1 Sv in 2015 to 13.2 Sv in 2017 with an averaged southward transport  
124 of  $13.9 \pm 1$  Sv. The uncertainties for transports indicated here and below are estimated as the  
125 standard deviation of their interannual variability.

126 Transports at  $26.5^\circ\text{N}$  are analysed from the repeated hydrographic sections of the World Ocean  
127 Circulation Experiments (WOCE) at line A05. The A05 section was occupied in summer 1992,  
128 1998, 2004, 2010, 2011 and, more recently, in 2015 (Bryden et al., 2005; Fu et al., 2020). At this  
129 section, the transport in the AMOC lower limb ranges from 12.3 Sv in 2004 to 18.2 Sv in 2010  
130 with an average southward transport over all years of  $15.9 \pm 2$  Sv.

## 131 *2.2 Hindcast simulation of the eddy-rich ocean model configuration, VIKING20X*

132 VIKING20X is an eddy-rich ocean/sea-ice coupled model configuration developed by GEOMAR  
133 (Biaostoch et al., 2021) and based on the version 3.6 of NEMO (“Nucleus for European Modeling  
134 of the Ocean”; Madec & NEMO-team, 2016). It is an updated and expanded version of the well-  
135 established VIKING20 configuration that is known for its good representation of the North  
136 Atlantic circulation (Böning et al., 2016; Handmann et al., 2018). In VIKING20X, the global  
137 horizontal resolution of  $1/4^\circ$  is refined over the full Atlantic Ocean ( $34^\circ\text{S}$ – $70^\circ\text{N}$ ) to a horizontal  
138 resolution of  $1/20^\circ$ . The vertical resolution is composed of 46 z-levels of 6 m at surface to a  
139 maximum of 250 m at depth, with partial bottom cells. The surface boundary conditions were  
140 constrained by realistic atmospheric forcing. Biaostoch et al. (2021) showed that the choice of the  
141 atmospheric forcing dataset is critical for a proper simulation of the AMOC variability. Indeed,  
142 the shift from COREv2 forcing (Griffies et al., 2009) to JRA55-do forcing (Tsujino et al., 2020)  
143 generally improved the velocity structures of the main currents in the North Atlantic. In this study,  
144 we thus use the 5-day mean velocity fields from the nested domain of a hindcast simulation from  
145 1980 to 2018 that uses the JRA55-do forcing. This simulation is referred to as VIKING20X-JRA-  
146 short.

### 147 *2.3 Definition of uNADW in VIKING20X-JRA-short*

148 In the following, we investigate the pathways and hydrographic property evolution of uNADW  
149 from OSNAP to 26.5°N as well as around the rim of the Labrador Sea. The layer excludes the  
150 overflow water from the Nordic Seas and is defined at  $\sigma_2 = 36.5\text{-}36.97 \text{ kg m}^{-3}$  (approx.  $\sigma_0 = 27.65\text{-}$   
151  $27.8 \text{ kg m}^{-3}$ ) in the observations at the Abaco line (Van Sebille et al., 2011) and at OSNAP (Li et  
152 al., 2021b). However, this definition needs to be adjusted in VIKING20X-JRA-short to account  
153 for a density bias of the model. For a hindcast simulation with VIKING20, Handmann et al. (2018)  
154 adjusted the density limits of the uNADW layer to  $\sigma_2 = 36.68\text{-}37.03 \text{ kg m}^{-3}$  in the central Labrador  
155 Sea. The upper limit is associated with the density of the maximum overturning at the OSNAP line  
156 in the model. The lower limit has been estimated by identifying the isopycnal with the lowest  
157 statistical depth variation. We use the same density limits to define the uNADW layer in  
158 VIKING20X-JRA-short because of a similar bias in density between the two models (not shown).

159 We use the terms “source” and “net formation” independently throughout our analysis to refer to  
160 the production of water into the uNADW layer, as defined by the density range  $\sigma_2 = 36.68\text{-}37.03$   
161  $\text{kg m}^{-3}$ , without considering specific classes of uNADW. We use the term “transformation” to refer  
162 to changes in hydrographic properties within the uNADW layer. Note that our experiments do not  
163 allow us to determine the specific mechanisms responsible for these net formations or  
164 transformations, which can be forced by air-sea interaction and/or by interior mixing.

165 Because the uNADW density at the exit of the subpolar gyre is highly variable in time (Yashayaev  
166 & Loder, 2016), we compare the uNADW properties of 2 specific periods (1991-1995 and 2014-  
167 2018; see section 2.4) within the isopycnals that bound the core of uNADW from 1980-2018 across  
168 the Labrador Current (LC) section. To identify these bounding isopycnals we compute the standard  
169 deviation of the density associated with the maximum transport at the LC section during this  
170 period. Hence, the core of uNADW is defined by the density range  $36.87\text{-}37.0 \text{ kg m}^{-3}$  in  
171 VIKING20X-JRA-short.

### 172 *2.4 Lagrangian experiments with ARIANE*

173 We use the software ARIANE (version 2.3) to perform two sets of Lagrangian experiments  
174 (Blanke & Raynaud, 1997; van Sebille et al., 2018). ARIANE computes particle trajectories in a  
175 time-varying three-dimensional velocity field. The particle trajectories can be interpreted as stream



176 tubes, allowing for the estimation of volume transports between the release and destination  
177 sections (e.g., van Sebille et al. 2018). The release section defines the starting point for the stream  
178 tubes, where the number of particles seeded by ARIANE is proportional to the transport field and  
179 can be restricted to a density layer. The evolution of the particle density along these trajectories is  
180 estimated by linearly interpolating the temperature and salinity fields at each position of the  
181 particle between neighbouring grid points. At the destination section, the volume flux of all  
182 particles arriving in a specific density bin are then summed to yield the total volume transport. In  
183 these experiments, the integration of the particle trajectories stops once the particle reaches a  
184 predefined destination section or once the maximum integration time is reached.

185 A first set of experiments, called EXP\_1, is designed to track particles of uNADW from 26.5°N  
186 back to the OSNAP sections, determine whether they are sourced from OSNAP East or OSNAP  
187 West, and record the along-track evolution of their hydrographic properties between the sections  
188 (Figure 1a). In EXP\_1, we perform 10 individual experiments where particles are released in the  
189 uNADW layer at 26.5°N (from coast to coast) every 5 days during every year of the 2009 to 2018  
190 period. These particles are then advected backward in time until they reach one of the destination  
191 sections, OSNAP East or OSNAP West, over the integration period. We use a maximum  
192 integration time of 78 years in order to have less than ~13% of particles ‘lost’ between the release  
193 and destination sections. To achieve this integration time, we loop twice through the velocity field  
194 of the 1980-2018 period. Although a loop can introduce unrealistic jumps in the evolution of the  
195 hydrographic properties (Döös et al., 2008; Thomas et al., 2015), the error in the along-track  
196 property of the particles is negligible in this analysis due to the high number of particles seeded  
197 (i.e.,  $O(10^5)$  per experiment) and to the small drift in temperature and salinity observed in the  
198 model during this period (i.e., trends of  $-0.0014^{\circ}\text{C}$  and  $-0.0114$  psu over the nest and for the entire  
199 water column). Moreover, Figure S1 shows that the density changes at the looping point for the  
200 particles seeded in EXP\_1 are small in comparison to their density changes between the release  
201 and destination sections.

202 The second set of experiments, called EXP\_2, is designed to back track particles of uNADW from  
203 the LC section to the West Greenland Current (WGC) section and analyse the evolution of their  
204 hydrographic properties within the Labrador Sea (Figure 1a). In EXP\_2, we release particles in the  
205 uNADW layer at the LC section every 5 days during every year of the OSNAP period (2014-

206 2018). The particles are then advected backward in time until they reach the WGC section in a  
207 maximum of 5 years. A maximum integration time of 5 years is sufficient because only 1% of the  
208 particles remain in the Labrador Sea after 5 years of integration. However, as the OSNAP period  
209 is associated with a relatively weak uNADW export through the LC section (Figure 1b), the EXP\_2  
210 is additionally performed over the period 1991-1995, which exhibits a relatively strong uNADW  
211 export. Note that the particles considered in EXP\_2 are not a subset of the particles released of  
212 EXP\_1 because of the difference in the time periods considered.

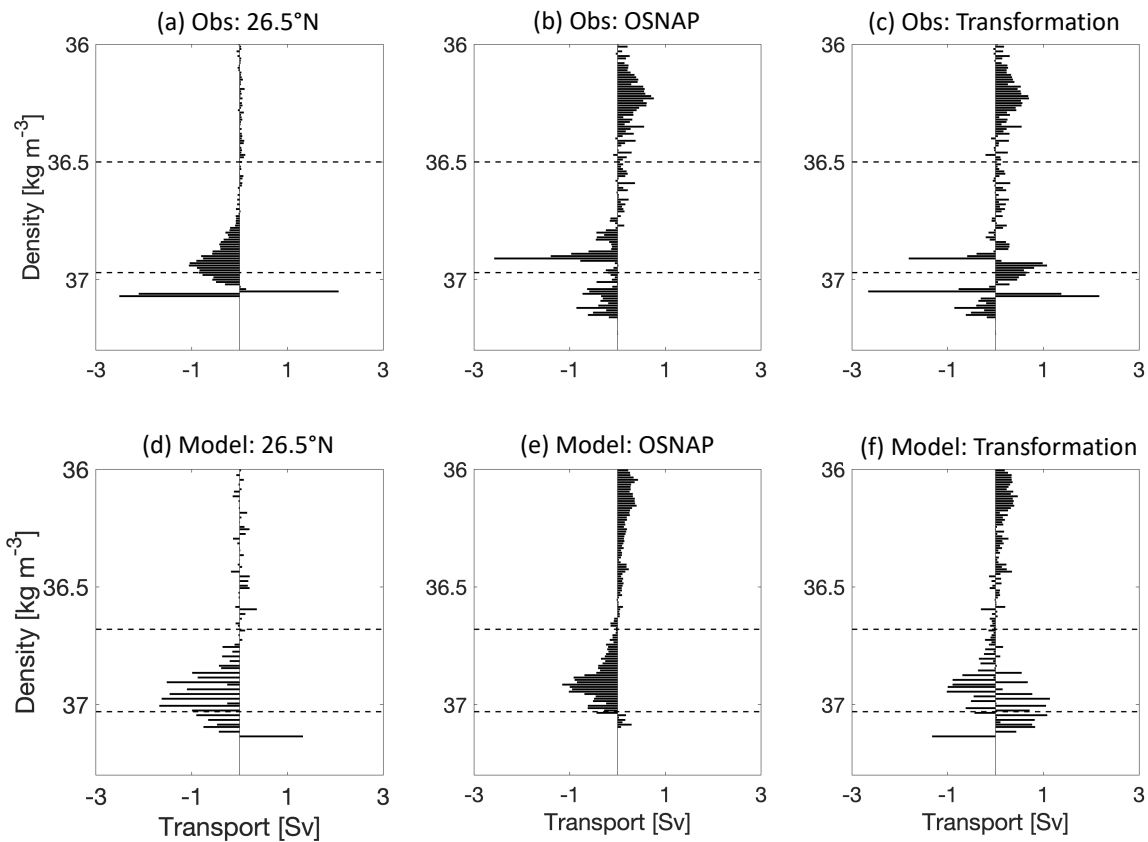
### 213 *2.5 Model evaluation: Eulerian transformation of uNADW*

214 Biastoch et al. (2021) showed that the large-scale horizontal circulation of the North Atlantic, the  
215 deep water transport in the boundary current, as well as the mean structure and variability of the  
216 AMOC are well simulated in VIKING20X-JRA-short as compared to observations. For instance,  
217 a major part of the overturning occurs at OSNAP East instead of OSNAP West in the model, which  
218 is consistent with OSNAP observations. A good representation of the convective processes in the  
219 subpolar North Atlantic, including the shift of the convection from the Labrador to the Irminger  
220 Sea in 2015–2018, was also highlighted by Rühls et al. (2021).

221 In this section, we further show that the uNADW transport at OSNAP and 26.5°N is well  
222 reproduced in the model. Indeed, Figure 2 shows the transport estimated per density bin of 0.01  
223 kg m<sup>-3</sup> at these two sections in both model and observations. The observational transports at  
224 OSNAP are averaged over the OSNAP period and those at the A05 section are an average of the  
225 3 occupations in the 2010s. Using the full temporal record of VIKING20X-JRA-short, we estimate  
226 that the bias introduced by the truncated observational time periods at the two sections is ~ 0.39  
227 Sv in the uNADW layer.

228 Overall, the structure of the transports across OSNAP and 26.5°N is consistent between the model  
229 and observations. The difference in transport between these two sections allows us to identify the  
230 transformation associated within each density bin, although it does not allow for a determination  
231 of the specific mechanism (e.g., buoyancy forcing and interior mixing) that create this  
232 transformation. The transformation between the sections shows a net increase in transport for  
233 subpolar mode water between 36.1-36.4 kg m<sup>-3</sup> and a net decrease in transport for overflow water  
234 denser than 37.0 kg m<sup>-3</sup> (Figures 2c, f). Though the transformation over the uNADW layer is highly

235 variable in density, there is a net increase of 3.1 Sv in the observations and of 4.0 Sv in  
 236 VIKING20X-JRA-short, which is mainly localized in the lower part of the layer. Because the  
 237 volume budget in the uNADW layer is remarkably consistent between the model and observations,  
 238 we are confident in the use of VIKING20X-JRA-short for our investigation of the uNADW  
 239 pathways between these sections.



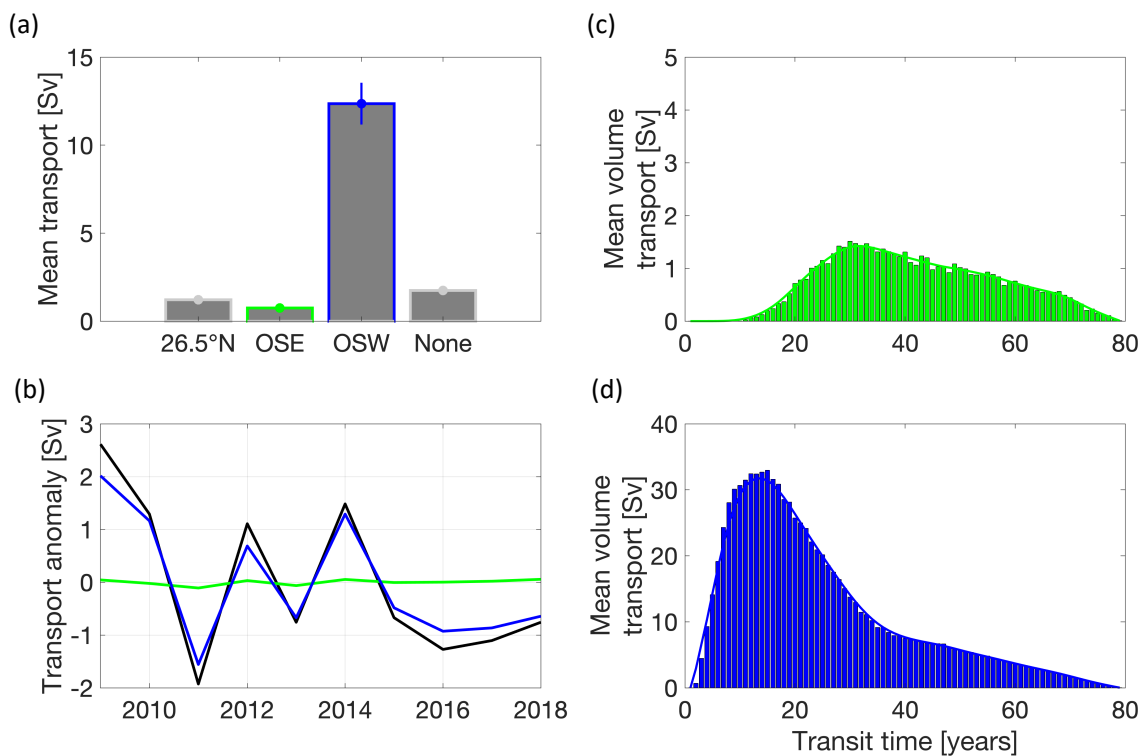
240

241 **Figure 2.** (a-c) Observed and (d-f) simulated transports (Sv) integrated in density bins of  $0.01 \text{ kg m}^{-3}$  at  $26.5^\circ\text{N}$   
 242 and OSNAP. Dashed lines indicate the potential density for the uNADW layer, with subpolar mode water and  
 243 overflow waters residing above and below this layer, respectively. In observations, the transports at OSNAP are  
 244 averaged during the 4 years of observations, while the transports at  $26.5^\circ\text{N}$  include the A05 sections in 2010,  
 245 2011 and 2015. Positive transports are northward. (c,f) Difference in transport between  $26.5^\circ\text{N}$  and OSNAP.  
 246 Positive (negative) transformation is associated with net increase (decrease) of transport in the respective density  
 247 bin between the two sections.

### 248 3. Source and transformation of uNADW from OSNAP to $26.5^\circ\text{N}$

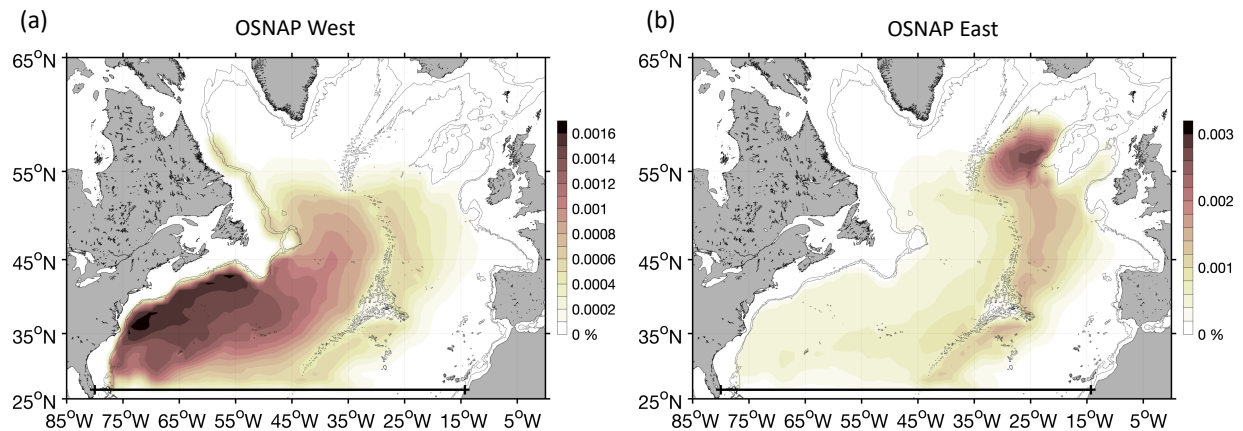
249 The pathways and net property evolution of uNADW observed at  $26.5^\circ\text{N}$  are analyzed with the  
 250 Lagrangian experiments EXP\_1. At the release section, the particles seeded in the uNADW layer  
 251 are mainly localized along the western boundary of the section ( $52.5\text{-}53.5^\circ\text{W}$ ) and associated with

252 a relatively strong transport for densities  $> 36.85 \text{ kg m}^{-3}$  (Figure S2). After accounting for the  $\sim 55$   
 253 Sv of particles that recirculate southward across the release section, we track a total of 16.1 Sv of  
 254 particles to their destination over the integration time period. The upstream distribution of these  
 255 particles (Figure 3a) reveals that they are largely advected from OSNAP West (12.4 Sv or 77%),  
 256 mainly along the western boundary of the section (Figure S2c), rather than from OSNAP East (0.7  
 257 Sv or 4.6%). The interannual variability of the transport at  $26.5^\circ\text{N}$  (Figure 3b) is also dominated  
 258 by the OSNAP West contributions. As for other sources, 1.8 Sv does not reach a section during  
 259 the integration time and is considered “lost” in the study area, mainly east of the Mid-Atlantic  
 260 Ridge (not shown), and 1.2 Sv recirculates across the release section in an adjoining density layer.  
 261 Therefore, the main source for uNADW at  $26.5^\circ\text{N}$  is OSNAP West, which suggests that uNADW  
 262 sourced from the eastern subpolar gyre is mainly advected through the Labrador Sea instead of  
 263 being directly advected from OSNAP East through interior pathways.



264  
 265 **Figure 3.** Sources for uNADW deduced from the set of experiments EXP\_1. (a) Mean volumetric contributions  
 266 of the individual sources to uNADW at  $26.5^\circ\text{N}$ . Dots and lines indicate the mean and standard deviation of the  
 267 transport over the 10 experiments, respectively. (b) Interannual variability of the total uNADW transport  
 268 anomaly (black) and its individual contributions OSNAP East (OSE in green) and OSNAP West (OSW in blue)  
 269 estimated with the 10 different release years. (c-d) Transit times for the particles to reach  $26.5^\circ\text{N}$  from the  
 270 destination sections (c) OSNAP East and (d) OSNAP West. Bars indicate the mean transit time distributions for  
 271 the set of 10 experiments and the lines indicate the distribution smoothed using a 5-points moving average.

272 The transit times of the particles advected from OSNAP West show that more than 50% reach  
 273 26.5°N in 20 years, with the highest number of particles (modal value) reaching the section after  
 274 14 years (Figure 3d). The advective transit time of the particles from OSNAP East is twice larger  
 275 than from OSNAP West. Indeed, the majority of particles from OSNAP East reach 26.5°N in 40  
 276 years with the highest number of particles reaching the section after 31 years (Figure 3c). The  
 277 difference in advective transit time between the two source sections is time invariant and is  
 278 explained by different uNADW pathways.

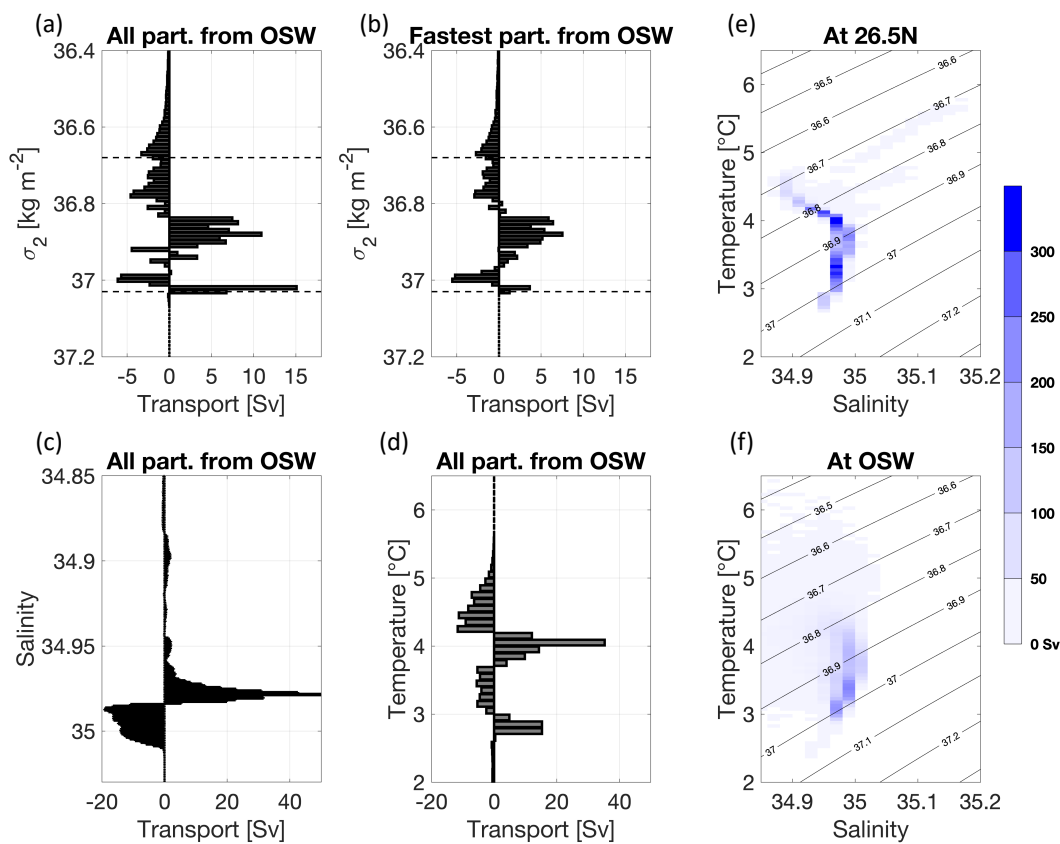


279  
 280 **Figure 4.** Dominant uNADW pathways between OSNAP and 26.5°N, from EXP\_1 for particle subsets reaching  
 281 (a) OSNAP West and (b) OSNAP East. The probability that a certain section is crossed by a particle during its  
 282 transit is estimated as the percentage of particle counts for each bin of a (0.5° x 0.5°) grid during the 2 cycles of  
 283 the experiment, such that the probabilities of all bins sum to 100%. Repeat crossings of a single particle are  
 284 included in the counts. The 10 individual probability distributions of each experiment in EXP\_1 are then  
 285 averaged. The black line shows the release section at 26.5°N.

286 The uNADW pathways between 26.5°N and OSNAP West, shown as a probability density  
 287 distribution in Figure 4a, reveal a myriad of pathways, including those in boundary current and in  
 288 the interior, consistent with past observational and modelling studies (Bower et al., 2009 and  
 289 Lozier et al. 2013). Nevertheless, the majority of the particles remain west of the Mid-Atlantic  
 290 Ridge instead of crossing the ridge eastward. On the contrary, the uNADW pathways between  
 291 26.5°N and OSNAP East are mainly restricted to the eastern side of the Mid-Atlantic Ridge (Figure  
 292 4b). The small fraction of particles that cross the ridge westward through deep fracture zones (e.g.  
 293 the Charlie Gibbs Fracture Zone and other deep fractures further south) preferentially follow its  
 294 western flank rather than the western boundary current. Therefore, the Mid-Atlantic Ridge acts as  
 295 a barrier in the propagation of uNADW, such that the particles exiting the eastern subpolar gyre

296 mainly propagate along its eastern flank, while those exiting the western subpolar gyre mainly  
 297 propagate to the west of the ridge.

298 Moreover, all particles coming from OSNAP East leave the eastern subpolar gyre through the  
 299 Iceland Basin and Rockall Trough instead of the Irminger Sea. Hence, uNADW sourced from the  
 300 Irminger Sea is not directly advected southward via interior pathways but is instead advected  
 301 westward through the Labrador Sea. These results are consistent with a recent study that details  
 302 the different Lagrangian pathways of the overflow waters from the Irminger and Labrador basin  
 303 compared to the Iceland basin (Lozier et al., 2022).



304

305 **Figure 5.** Thermohaline properties of uNADW reaching OSNAP West from the set of experiments EXP\_1. (a-  
 306 d) Difference in mean volume transport between the release section 26.5°N and the destination section OSNAP  
 307 West. The volume transport is estimated per (a-b) density bins of 0.01 kg m<sup>-3</sup>, (c) salinity bins of 0.001 and (d)  
 308 temperature bins of 0.1°C. Panel (d) includes only the 50% fastest particles reaching OSNAP West. Positive  
 309 (negative) transformation is associated with net increase (decrease) of transport in the respective density bin  
 310 from OSNAP West to 26.5°N. Dashed lines indicate the potential density  $\sigma_2 = 36.68$  and  $37.03$  kg m<sup>-3</sup> for the  
 311 uNADW layers in VINKING20X. (e-f) Volume transport (Sv) in each temperature and salinity bin at (e) the  
 312 release section and the (f) destination section.

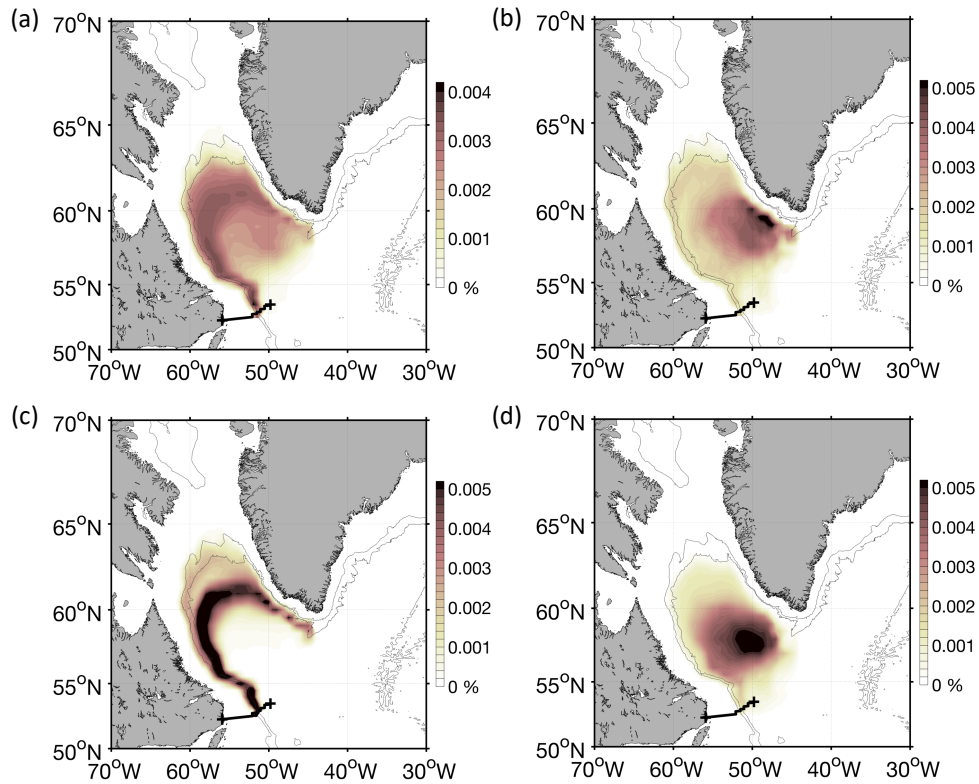
313 The property transformation of uNADW is now analyzed for particles advected between OSNAP  
314 West and 26.5°N. With our convention, a positive (negative) transformation is associated with net  
315 increase (decrease) of transport in the respective density range from OSNAP West to 26.5°N. A  
316 net increase of only 1.1 Sv is found in the uNADW layer between the sections, such that  $96.9 \pm$   
317  $0.4$  % of the particles belong to the uNADW density range at both the release and destination  
318 sections. However, there are large density changes within the uNADW layer (Figure 5a). In  
319 particular, we note a net increase in uNADW transport between 36.84 to 36.91 kg m<sup>-3</sup> and at 37.02  
320 kg m<sup>-3</sup>, and a net decrease in uNADW transport between 36.91 to 37.02 kg m<sup>-3</sup> and at  $\sigma_2 < 36.84$   
321 kg m<sup>-3</sup>. The uNADW densification is associated with a freshening from  $\sim 35$  to  $\sim 34.98$  and a  
322 cooling from  $\sim 4.5^\circ\text{C}$  to  $\sim 4^\circ\text{C}$  and at  $\sim 2.8^\circ\text{C}$  (Figures 5 c-d). The temperature/salinity diagrams at  
323 the two sections in Figures 5 (e-f) confirm that these transformations in salinity and temperature  
324 are mainly localized within the uNADW layer.

325 By comparing these transformations with those estimated for a subclass of particles, we find that  
326 the transformations in the density range of 36.68-36.91 kg m<sup>-3</sup> are mainly attributed to the 50%  
327 fastest particles (Figure 5b). Considering that these fast particles preferentially follow the boundary  
328 current, the transformation is possibly explained by the relatively strong gradient between the  
329 boundary current and the interior. However, the net increase in uNADW transport at 37.02 kg m<sup>-3</sup>  
330 is mainly attributed to particles remaining in the basin for more than 20 years, implying that  
331 particles reaching 26.5°N in more than 20 years play a role in the transformation of only the very  
332 dense uNADW.

#### 333 **4. Transformation of uNADW in the Labrador Sea**

334 Since the Labrador Sea is a key pathway for uNADW formed over the eastern subpolar gyre, we  
335 now investigate whether uNADW is further modified as it passes through the Labrador Sea. We  
336 first use the EXP\_2 performed during 2014-2018. In this set of experiments, nearly all the particles  
337 released at the LC section are advected from the WGC section, and more than 60% of the particles  
338 reach the destination section after only 1 year. This time scale is consistent with previous studies  
339 that document a transit time along the boundary current of the Labrador Sea of 1-2 years (Bower  
340 et al., 2009; Feucher et al., 2019; Georgiou et al., 2020) and with Lagrangian experiments that  
341 tracked backward in time overflow water from the Denmark Strait to 53°N in VIKING20X-JRA-  
342 OMIP (Fröhle et al., 2022).

343 During its transit through the Labrador Sea, the uNADW largely follows the boundary current in  
 344 the basin (Figure 6a). This pathway is particularly clear for particles reaching the destination  
 345 section in less than 1 year (Figure 6c). On the contrary, the particles reaching the destination  
 346 section in more than 4 years recirculate in the interior of the basin (Figure 6d). This area is  
 347 associated with deep mixed layer depths during wintertime, which were relatively deeper in the  
 348 90s than during the OSNAP period (Rühs et al., 2021).



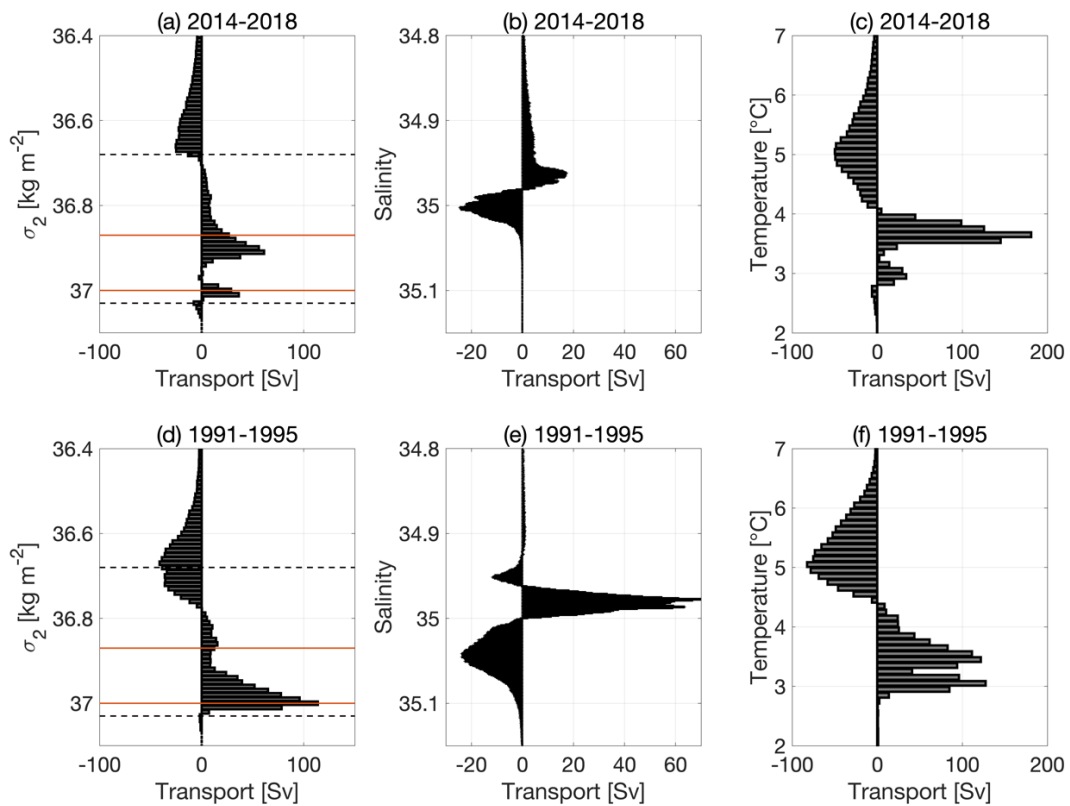
349  
 350 **Figure 6.** Probability distribution from EXP\_2 performed during 2014-2018 for (a) all the particles released at  
 351 the LC and for 3 subclasses of the experiment: (b) particles with a densification higher than  $0.1 \text{ kg m}^{-3}$  between  
 352 the release and destination sections, (c) particles reaching the destination section in less than 1 year, (d) particles  
 353 reaching the destination section in more than 4 years. The 4 individual probability distributions are estimated as  
 354 described in Figure 4 and are then averaged together. The black line shows the release section at the LC.  
 355 Bathymetry is contoured at 1000 m and 2000 m.

356 The difference in the density, salinity and temperature transformation along these pathways  
 357 between the 5-year period of relatively strong (1991-1995) and the 5-year period of relatively weak  
 358 (2014-2018) uNADW export is next examined. During the 2014-2018 period, 31.7% of subpolar  
 359 mode water is transformed into uNADW over the Labrador Sea (Figure 7a). During the 1991-1995  
 360 period, only 21.0% is transformed (Figure 7d). For both time periods, the boundary-following



361 particles that are in the Labrador Sea for less than one year account for most of the transformation  
 362 (Figures S3 and 6c). The difference in the proportion of subpolar mode water transformed into  
 363 uNADW (e.g. which is equivalent to the net volume of uNADW production as compared to the  
 364 outflowing volume of uNADW across OSNAP West) between the 2 periods is explained by the  
 365 vertical density structure of the inflowing water. The inflowing water is evenly distributed between  
 366 the subpolar mode water and uNADW layers in 1991-1995, while it is mainly localized in the  
 367 subpolar mode water layer in 2014-2018. Thus, the strong buoyancy loss over the Labrador Sea  
 368 during the 1991-1995 period contributes to both the net volume of newly formed uNADW and to  
 369 further densification of uNADW within the layer.

370 However, although the net increase in uNADW transport is small during these 2 periods, the  
 371 particles undergo substantial freshening and cooling between the WGC and LC sections. In  
 372 particular, we note a cooling of water from  $\sim 4\text{-}6^\circ\text{C}$  to  $\sim 3\text{-}4^\circ\text{C}$  (Figures 7c, f) and a freshening in  
 373 salinity from  $\sim 34.99\text{-}35.1$  to  $\sim 34.97$  (Figures 7b, e). These transformations are larger during the  
 374 strong convection period of the 90s than during the OSNAP period.



375

376 **Figure 7.** Difference in mean volume transport between the release section LC and the destination section WGC  
377 from the set of experiments EXP\_2 performed during (a-c) 2014-2018 and (d-f) 1991-1995. The volume  
378 transport is estimated per (a, d) density bins of  $0.01 \text{ kg m}^{-3}$ , (b, e) salinity bins of 0.001 psu and (c, f) temperature  
379 bins of  $0.1^\circ\text{C}$ . Positive transformation is associated with a net increase of transport in the respective density bin  
380 over the Labrador Sea. Dashed lines indicate the potential density  $\sigma_2 = 36.68$  and  $37.03 \text{ kg m}^{-3}$  for the uNADW  
381 layers in VIKING20X. Red lines indicate the limits in density for the uNADW core in the LC specifically.

382 Consequently, Figures 7a and 7d show that the uNADW formed in 1991-1995 (with a density peak  
383 at  $\sim 37 \text{ kg m}^{-3}$ ) spans the densest part of the averaged core of uNADW, as identified by the red  
384 lines, while the uNADW formed in 2014-2018 (with a density peak at  $\sim 36.91 \text{ kg m}^{-3}$ ) spans its  
385 lightest part. Most of this transformation occurs within the uNADW layer to particles remaining  
386 in the center of the Labrador Sea for more than 1 year (Figures S3 and 6d). In agreement with  
387 previous studies (Jackson et al., 2016; Yashayaev & Loder, 2016), we thus show that the uNADW  
388 transformed in the Labrador Sea is denser in the 90s than during the OSNAP period. Therefore,  
389 the strength of the convection in the Labrador Sea influences the changes in uNADW properties  
390 within the AMOC lower limb.

391 Finally, we show that the largest density changes (greater than  $0.1 \text{ kg m}^{-3}$  in Figure 6b) are mainly  
392 localized along the West Greenland Current between Eirik Ridge and Cape Desolation, which is  
393 where the Irminger Rings are shed and recirculation takes place (Cuny et al., 2002), instead of the  
394 interior of the basin. This agrees well with previous studies revealing the importance of density  
395 changes along the boundary current for the dynamic of the subpolar gyre (Menary et al., 2020;  
396 Spall, 2004; Straneo, 2006), as well as with a recent study (Fröhle et al., 2022) showing that  
397 uNADW formation in the Labrador Sea on decadal time scales is mainly a result of diapycnal mass  
398 fluxes over this area rather than by mixed layer formation over the interior of the basin.

399 To summarize, the Labrador Sea is not associated with large uNADW formation, but is a key  
400 pathway for uNADW sourced over the eastern subpolar gyre and is a key location for uNADW  
401 densification within the AMOC lower limb.

## 402 **5. Conclusion and discussion**

403 In this study, the mean pathways and along-stream transformation of uNADW from OSNAP to  
404  $26.5^\circ\text{N}$  are investigated using Lagrangian experiments performed in a hindcast simulation with the  
405 eddy-rich ocean model VIKING20X-JRA-short. In order to better understand the sources of  
406 transport and density anomalies of uNADW that are observed at  $26.5^\circ\text{N}$ , particles were released

407 at 26.5°N and advected backward in time until they reached the OSNAP East or OSNAP West  
408 sections. In this first set of experiments, we show that OSNAP West is the main source section for  
409 uNADW (77%), and that a large majority of uNADW at 26.5°N trace back from the Labrador Sea  
410 instead of being directly advected from OSNAP East through interior pathways.

411 In particular, we show that all the particles advected southward from OSNAP East without a detour  
412 in the Labrador Sea leave the eastern subpolar gyre from the Iceland Basin and Rockall Trough  
413 rather than from the Irminger Sea. The Labrador Sea is thus the main gateway for uNADW from  
414 the Irminger Sea to the subtropical latitudes. This advective pathway compares well with the  
415 observed propagation pathways of the underlying overflow water shown by Lozier et al. (2022),  
416 where 94% of their floats enter the Labrador Sea despite the sharply curved Eirik Ridge.

417 Although only a small volume of uNADW is directly advected from OSNAP East to 26.5°N, we  
418 further show that the particles from the Iceland Basin and Rockall Trough do not follow the  
419 boundary current but propagate southward along the eastern flank of the Mid-Atlantic Ridge. This  
420 southward pathway is consistent with the observed spread of overflow water from the Iceland  
421 Basin (Lozier et al., 2022) and has been estimated to contribute to  $38 \pm 14$  % of the whole basin  
422 meridional transport from 50°N to 35°N (Zhai et al., 2021). Its propagation is possibly explained  
423 by the mesoscale activity of the North Atlantic Current at the entrance of the basin, which is known  
424 to divert deep water eastward at the Charlie-Gibbs Fracture Zone (Zou et al., 2020b).

425 On the contrary, the particles reaching 26.5°N from OSNAP West follow both the boundary  
426 current and interior pathways west of the Mid-Atlantic Ridge. The distribution of the interior  
427 pathways agrees well with the observed LSW pathways from Argo floats shown by Biló & Johns  
428 (2019), and can partially delay the propagation of uNADW anomalies between the sections  
429 (Chomiak et al., 2022). The uNADW anomalies are, indeed, commonly used to infer advective  
430 timescales between the Labrador Sea and 26.5°N. However, we show that the uNADW exported  
431 from the Labrador Sea is modified along these pathways. Indeed, although the transport in the  
432 uNADW layer increases by only 1.1 Sv between OSNAP West and 26.5°N, we highlight that these  
433 pathways are associated with large temperature and salinity changes within the uNADW layer.  
434 The mechanism of transformation between the subpolar and subtropical gyres could be due to  
435 entrainment of dense water between the boundary current and/or the interior or by mixing with  
436 surrounding water during recirculation within the subpolar gyre. Further investigation, however,

437 is needed to reveal the relative importance of these different densification processes and of their  
438 temporal variability.

439 During the transit through the Labrador Sea, the second set of experiments shows only a small  
440 increase of transport in the uNADW layer, which is slightly more pronounced in 2014-2018  
441 (31.7%) than in 1991-1995 (21.0%). However, although the uNADW formation is small during  
442 these 2 periods, we show that strong convection years (1991-1995) lead to large changes in salinity  
443 and temperature that drive uNADW densification within the AMOC lower limb. This is consistent  
444 with the density compensated overturning shown by Zou et al. (2020a) in the Labrador Sea. Thus,  
445 the buoyancy loss over the Labrador Sea contributes to both the net volume of newly formed  
446 uNADW for particles remaining less than 1 year in the basin and to a further densification of  
447 uNADW within the layer for particles remaining more than 1 year in the basin. These two (indirect  
448 and direct) routes and the associated difference in residence time scale are consistent with  
449 Georgiou et al. (2021) which showed that the indirect route governs the transformation within the  
450 denser layers.

451 In addition, it has been shown that the circulation of the subpolar gyre can be influenced by changes  
452 in the dynamics of the boundary current. An increase in the interior deep convection of the  
453 Labrador Sea would lead to an increase in the radial density gradient and, thus, to a stronger  
454 baroclinic flow along the boundary current (Straneo, 2006; Born & Stocker, 2014; Ghosh et al.,  
455 2023).

456 These two mechanisms imply that, although Labrador Sea convection is not the primary source  
457 for the lower limb of the AMOC, the strength of convection in the Labrador Sea could influence  
458 the AMOC by modifying the properties of the uNADW that propagates downstream to 26.5°N  
459 and, possibly, the uNADW that flows from the Labrador Sea to the eastern subpolar gyre via  
460 recirculation pathways. This is consistent with previous studies showing that eastward  
461 recirculation is important for setting the hydrography of the eastern subpolar gyre at both  
462 interannual (Asbjørnsen et al., 2021; Fox et al., 2022; Holliday et al., 2020) and decadal timescales  
463 (Yeager et al., 2021). The impact of these modified uNADW properties for the AMOC through  
464 recirculation in the subpolar gyre is beyond the scope of our analysis and is the purpose of a follow-  
465 up study.

466 **Acknowledgements**

467 T.P. and M.S.L. acknowledge support from the National Science Foundation Physical  
468 Oceanography Program (NSF OCE-1948335). T.P. was also funded by the NERC SNAP-  
469 DRAGON project (NE/T013494/1). For the purpose of open access, the author has applied a  
470 'Creative Commons Attribution (CC BY)' licence to any Author Accepted Manuscript version  
471 arising.

472 **Open Research**

473 The OSNAP data used for this work are available online at [https://www.o-](https://www.osnap.org/observations/data/)  
474 [snap.org/observations/data/](https://www.osnap.org/observations/data/) (Fu et al, 2023a) (Fu et al, 2023b).

475 **References**

- 476 Asbjørnsen, H., Johnson, H. L., & Arthun, M. (2021). Variable Nordic Seas Inflow Linked to  
477 Shifts in North Atlantic Circulation. *Journal of Climate*, 34(17), 7057–7071.  
478 <https://doi.org/10.1175/JCLI-D-20-0917.1>
- 479 Biastoch, A., Schwarzkopf, F. U., Getzlaff, K., Rühls, S., Martin, T., Scheinert, M., et al. (2021).  
480 Regional imprints of changes in the Atlantic Meridional Overturning Circulation in the  
481 eddy-rich ocean model VIKING20X. *Ocean Science*, 17(5), 1177–1211.  
482 <https://doi.org/10.5194/os-17-1177-2021>
- 483 Biló, T. C., & Johns, W. E. (2019). Interior Pathways of Labrador Sea Water in the North  
484 Atlantic From the Argo Perspective. *Geophysical Research Letters*, 46(6), 3340–3348.  
485 <https://doi.org/10.1029/2018GL081439>
- 486 Blanke, B., & Raynaud, S. (1997). Kinematics of the Pacific Equatorial Undercurrent: An  
487 Eulerian and Lagrangian approach from GCM results. *Journal of Physical Oceanography*,  
488 27(6), 1038–1053. [https://doi.org/10.1175/1520-0485\(1997\)027<1038:KOTPEU>2.0.CO;2](https://doi.org/10.1175/1520-0485(1997)027<1038:KOTPEU>2.0.CO;2)
- 489 Böning, C. W., Behrens, E., Biastoch, A., Getzlaff, K., & Bamber, J. L. (2016). Emerging impact  
490 of Greenland meltwater on deepwater formation in the North Atlantic Ocean. *Nature*  
491 *Geoscience*, 9(7), 523–527. <https://doi.org/10.1038/ngeo2740>
- 492 Born, A., and T. F. Stocker, 2014: Two Stable Equilibria of the Atlantic Subpolar Gyre. *J. Phys.*  
493 *Oceanogr.*, 44, 246–264, <https://doi.org/10.1175/JPO-D-13-073.1>
- 494 Bower, A. S., Lozier, M. S., Gary, S. F., & Böning, C. W. (2009). Interior pathways of the North  
495 Atlantic meridional overturning circulation. *Nature*, 459(7244), 243–247.  
496 <https://doi.org/10.1038/nature07979>
- 497 Bryden, H. L., Longworth, H. R., & Cunningham, S. A. (2005). Slowing of the Atlantic  
498 meridional overturning circulation at 25° N. *Nature*, 438(7068), 655–657.  
499 <https://doi.org/10.1038/nature04385>
- 500 Chafik, L., & Rossby, T. (2019). Volume, Heat, and Freshwater Divergences in the Subpolar  
501 North Atlantic Suggest the Nordic Seas as Key to the State of the Meridional Overturning  
502 Circulation. *Geophysical Research Letters*, 46(9), 4799–4808.  
503 <https://doi.org/10.1029/2019GL082110>
- 504 Chomiak, L. N., Yashayaev, I., Volkov, D. L., & Schmid, C. (2022). Inferring Advective  
505 Timescales and Overturning Pathways of the Deep Western Boundary Current in the North  
506 Atlantic Through Labrador Sea Water Advection *Journal of Geophysical Research : Oceans*,

507 1–23. <https://doi.org/10.1029/2022JC018892>

508 Cuny, J., Rhines, P. B., Niiler, P. P., & Bacon, S. (2002). Labrador Sea Boundary Currents and  
509 the Fate of the Irminger Sea Water. *Journal of Physical Oceanography*, 32(2), 627–647.  
510 [https://doi.org/10.1175/1520-0485\(2002\)032%3C0627:lsbeat%3E2.0.co;2](https://doi.org/10.1175/1520-0485(2002)032%3C0627:lsbeat%3E2.0.co;2)

511 Curry, R. G., McCartney, M. S., & Joyce, T. M. (1998). Linking subtropical deep water climate  
512 signals to North Atlantic subpolar convection variability. *Nature*, 391, 575–577.

513 Döös, K., Nycander, J., & Coward, A. C. (2008). Lagrangian decomposition of the Deacon Cell.  
514 *Journal of Geophysical Research*, 113(C7), C07028. <https://doi.org/10.1029/2007JC004351>

515 Feucher, C., Garcia-Quintana, Y., Yashayaev, I., Hu, X., & Myers, P. G. (2019). Labrador Sea  
516 Water Formation Rate and Its Impact on the Local Meridional Overturning Circulation.  
517 *Journal of Geophysical Research: Oceans*, 124(8), 5654–5670.  
518 <https://doi.org/10.1029/2019JC015065>

519 Fox, A. D., Handmann, P., Schmidt, C., Fraser, N., Rühs, S., Sanchez-Franks, A., et al. (2022).  
520 Exceptional freshening and cooling in the eastern subpolar North Atlantic caused by  
521 reduced Labrador Sea surface heat loss. *Ocean Science*, 18, 1507–1533,  
522 <https://doi.org/10.5194/os-18-1507-2022>

523 Fröhle, J., Handmann, P. V. K., Biastoch, A., & Kiel, C. (2022). Major sources of North Atlantic  
524 Deep Water in the subpolar North Atlantic from Lagrangian analyses in a high – resolution  
525 ocean model, (May), 1–33. Retrieved from <https://doi.org/10.5194/egusphere-2022-313>

526 Fu, Y., Lozier, M. S., Biló, T.C., Bower, A., Cunningham, S., Cyr, F., et al. (2023a). Meridional  
527 Overturning Circulation Observed by the Overturning in the Subpolar North Atlantic  
528 Program (OSNAP) Array from August 2014 to June 2020 [Dataset]. *Georgia Institute of*  
529 *Technology*. <http://doi.org/10.35090/GATECH/70342>

530 Fu, Y., Lozier, M.S., Biló, T.C. et al. Seasonality of the Meridional Overturning Circulation in  
531 the subpolar North Atlantic. *Commun Earth Environ* 4, 181 (2023b).  
532 <https://doi.org/10.1038/s43247-023-00848-9>

533 Fu, Y., Feili, L., Karstensen, J., & Wang, C. (2020). A stable Atlantic Meridional Overturning  
534 Circulation in a changing North Atlantic Ocean since the 1990s. *Science Advances*, 6(48).  
535 <https://doi.org/10.1126/sciadv.abc7836>

536 Georgiou, S., Ypma, S. L., Brüggemann, N., Sayol, J-M., van der Boog, C. G., Spence, P., et al.  
537 (2021). Direct and indirect pathways of convected water masses and their impacts on the  
538 overturning dynamics of the Labrador Sea. *Journal of Geophysical Research: Oceans*, 126,  
539 e2020JC016654. <https://doi.org/10.1029/2020JC016654>

540 Georgiou, S., Ypma, S. L., Brüggemann, N., Sayol, J. M., Pietrzak, J. D., & Katsman, C. A.  
541 (2020). Pathways of the water masses exiting the Labrador Sea: The importance of  
542 boundary–interior exchanges. *Ocean Modelling*, 150(November 2019), 101623.  
543 <https://doi.org/10.1016/j.ocemod.2020.101623>

544 Ghosh, R., and Coauthors, 2023: Two Distinct Phases of North Atlantic Eastern Subpolar Gyre  
545 and Warming Hole Evolution under Global Warming. *J. Climate*, 36, 1881–  
546 1894, <https://doi.org/10.1175/JCLI-D-22-0222.1>

547 Griffies, S. M., Biastoch, A., Böning, C., Bryan, F., Danabasoglu, G., Chassignet, E. P., et al.  
548 (2009). Coordinated Ocean-ice Reference Experiments (COREs). *Ocean Modelling*, 26(1–  
549 2), 1–46. <https://doi.org/10.1016/j.ocemod.2008.08.007>

550 Handmann, P., Fischer, J., Visbeck, M., Karstensen, J., Biastoch, A., Böning, C., & Patara, L.  
551 (2018). The Deep Western Boundary Current in the Labrador Sea From Observations and a  
552 High-Resolution Model. *Journal of Geophysical Research: Oceans*, 123(4), 2829–2850.

553 <https://doi.org/10.1002/2017JC013702>  
 554 Holliday, N. P., Bersch, M., Berx, B., Chafik, L., Cunningham, S., Florindo-López, C., et al.  
 555 (2020). Ocean circulation causes the largest freshening event for 120 years in eastern  
 556 subpolar North Atlantic. *Nature Communications*, *11*(1), 585.  
 557 <https://doi.org/10.1038/s41467-020-14474-y>  
 558 Jackson, L. C., Peterson, K. A., Roberts, C. D., & Wood, R. A. (2016). Recent slowing of  
 559 Atlantic overturning circulation as a recovery from earlier strengthening. *Nature*  
 560 *Geoscience*, *9*(7), 518–522. <https://doi.org/10.1038/ngeo2715>  
 561 Koelling, J., Atamanchuk, D., Karstensen, J., Handmann, P., & Wallace, D. W. R. (2022).  
 562 Oxygen export to the deep ocean following Labrador Sea Water formation. *Biogeosciences*,  
 563 *19*(2), 437–454. <https://doi.org/10.5194/bg-19-437-2022>  
 564 Kostov, Y., Messias, M.-J., Mercier, H., Johnson, H. L., & Marshall, D. P. (2022). Fast  
 565 mechanisms linking the Labrador Sea with subtropical Atlantic overturning. *Climate*  
 566 *Dynamics*, (0123456789). <https://doi.org/10.1007/s00382-022-06459-y>  
 567 Li, F., Lozier, M. S., Holliday, N. P., Johns, W. E., Le Bras, I. A., Moat, B. I., et al. (2021a).  
 568 Observation-based estimates of heat and freshwater exchanges from the subtropical North  
 569 Atlantic to the Arctic. *Progress in Oceanography*, *197*(July), 102640.  
 570 <https://doi.org/10.1016/j.pocean.2021.102640>  
 571 Li, F., Lozier, M. S., Bacon, S., Bower, A. S., Cunningham, S. A., de Jong, M. F., et al. (2021b).  
 572 Subpolar North Atlantic western boundary density anomalies and the Meridional  
 573 Overturning Circulation. *Nature Communications*, *12*(1), 1–9.  
 574 <https://doi.org/10.1038/s41467-021-23350-2>  
 575 Li, Feili, Lozier, M. S., & Johns, W. E. (2017). Calculating the meridional volume, heat, and  
 576 freshwater transports from an observing system in the subpolar North Atlantic: Observing  
 577 system simulation experiment. *Journal of Atmospheric and Oceanic Technology*, *34*(7),  
 578 1483–1500. <https://doi.org/10.1175/JTECH-D-16-0247.1>  
 579 Lozier, M. S., Li, F., Bacon, S., Bahr, F., Bower, A. S., Cunningham, S. A., et al. (2019). A sea  
 580 change in our view of overturning in the subpolar North Atlantic. *Science*, *363*(6426), 516–  
 581 521. <https://doi.org/10.1126/science.aau6592>  
 582 McCartney, M. S., & Talley, L. D. (1982). The Subpolar Mode Water of the North Atlantic.  
 583 *Journal of Physical Oceanography*, *12*, 1169–1188.  
 584 Menary, M. B., Jackson, L. C., & Lozier, M. S. (2020). Reconciling the relationship between the  
 585 AMOC and Labrador Sea in OSNAP observations and climate models. *Geophysical Research*  
 586 *Letters*, *47*, e2020GL089793. <https://doi.org/10.1029/2020GL089793>  
 587 Molinari, R. L., Fine, R. A., Wilson, W. D., Curry, R. G., Abell, J., & McCartney, M. S. (1998).  
 588 The arrival of recently formed Labrador sea water in the Deep Western Boundary Current at  
 589 26.5°N. *Geophysical Research Letters*, *25*(13), 2249–2252.  
 590 <https://doi.org/10.1029/98GL01853>  
 591 Petit, T., Lozier, M. S., Josey, S. A., & Cunningham, S. A. (2020). Atlantic Deep Water  
 592 Formation Occurs Primarily in the Iceland Basin and Irminger Sea by Local Buoyancy  
 593 Forcing. *Geophysical Research Letters*, *47*(22), 1–9.  
 594 <https://doi.org/10.1029/2020GL091028>  
 595 Pickart, R. S., Straneo, F., & Moore, G. W. K. (2003). Is Labrador Sea Water formed in the  
 596 Irminger basin? *Deep-Sea Research Part I: Oceanographic Research Papers*, *50*(1), 23–52.  
 597 [https://doi.org/10.1016/S0967-0637\(02\)00134-6](https://doi.org/10.1016/S0967-0637(02)00134-6)  
 598 Rhein, M., Fischer, J., Smethie, W. M., Smythe-Wright, D., Weiss, R. F., Mertens, C., et al.



599 (2002). Labrador Sea Water: Pathways, CFC Inventory, and Formation Rates. *Journal of*  
600 *Physical Oceanography*, 32(2), 648–665. [https://doi.org/10.1175/1520-](https://doi.org/10.1175/1520-0485(2002)032<0648:LSWPCI>2.0.CO;2)  
601 [0485\(2002\)032<0648:LSWPCI>2.0.CO;2](https://doi.org/10.1175/1520-0485(2002)032<0648:LSWPCI>2.0.CO;2)

602 Rühls, S., Oliver, E. C. J., Biastoch, A., Böning, C. W., Dowd, M., Getzlaff, K., et al. (2021).  
603 Changing Spatial Patterns of Deep Convection in the Subpolar North Atlantic. *Journal of*  
604 *Geophysical Research: Oceans*, 126(7), 1–24. <https://doi.org/10.1029/2021JC017245>

605 van Sebille, E., Griffies, S. M., Abernathey, R., Adams, T. P., Berloff, P., Biastoch, A., et al.  
606 (2018). Lagrangian ocean analysis: Fundamentals and practices. *Ocean Modelling*,  
607 121(October 2017), 49–75. <https://doi.org/10.1016/j.ocemod.2017.11.008>

608 Van Sebille, E., Baringer, M. O., Johns, W. E., Meinen, C. S., Beal, L. M., De Jong, M. F., &  
609 Van Aken, H. M. (2011). Propagation pathways of classical Labrador Sea water from its  
610 source region to 26°N. *Journal of Geophysical Research: Oceans*, 116(12), 1–18.  
611 <https://doi.org/10.1029/2011JC007171>

612 Spall, M. A., 2004: Boundary Currents and Watermass Transformation in Marginal Seas. *J.*  
613 *Phys. Oceanogr.*, 34, 1197–1213,  
614 [https://doi.org/10.1175/15200485\(2004\)034<1197:BCAWTI>2.0.CO;2](https://doi.org/10.1175/15200485(2004)034<1197:BCAWTI>2.0.CO;2)

615 Straneo, F., 2006: On the Connection between Dense Water Formation, Overturning, and  
616 Poleward Heat Transport in a Convective Basin. *J. Phys. Oceanogr.*, 36, 1822–  
617 1840, <https://doi.org/10.1175/JPO2932.1>

618 Straneo, F., Pickart, R. S., & Lavender, K. (2003). Spreading of Labrador sea water: An  
619 advective-diffusive study based on Lagrangian data. *Deep-Sea Research Part I:*  
620 *Oceanographic Research Papers*, 50(6), 701–719. [https://doi.org/10.1016/S0967-](https://doi.org/10.1016/S0967-0637(03)00057-8)  
621 [0637\(03\)00057-8](https://doi.org/10.1016/S0967-0637(03)00057-8)

622 Susan Lozier, M., Bower, A. S., Furey, H. H., Drouin, K. L., Xu, X., & Zou, S. (2022). Overflow  
623 Water Pathways in the North Atlantic. *Progress in Oceanography*, 208(June), 102874.  
624 <https://doi.org/10.1016/j.pocean.2022.102874>

625 Thomas, M. D., Tréguier, A.-M., Blanke, B., Deshayes, J., & Voldoire, A. (2015). A Lagrangian  
626 Method to Isolate the Impacts of Mixed Layer Subduction on the Meridional Overturning  
627 Circulation in a Numerical Model. *Journal of Climate*, 28(19), 7503–7517.  
628 <https://doi.org/10.1175/JCLI-D-14-00631.1>

629 Tooth, O. J., Johnson, H. L., & Wilson, C. (2022). Lagrangian Overturning Pathways in the  
630 Eastern Subpolar North Atlantic. *Journal of Climate*, (2019), 1–53.  
631 <https://doi.org/10.1175/jcli-d-21-0985.1>

632 Tsujino, H., Urakawa, L. S., Griffies, S. M., Danabasoglu, G., Adcroft, A. J., Amaral, A. E., et  
633 al. (2020). Evaluation of global ocean–sea-ice model simulations based on the experimental  
634 protocols of the Ocean Model Intercomparison Project phase 2 (OMIP-2). *Geoscientific*  
635 *Model Development*, 13(8), 3643–3708. <https://doi.org/10.5194/gmd-13-3643-2020>

636 Yashayaev, I., & Loder, J. W. (2016). Recurrent replenishment of Labrador Sea Water and  
637 associated decadal-scale variability. *Journal of Geophysical Research: Oceans*, 121(11),  
638 8095–8114. <https://doi.org/10.1002/2016JC012046>

639 Yashayaev, I., Bersch, M., & van Aken, H. M. (2007). Spreading of the Labrador Sea Water to  
640 the Irminger and Iceland basins. *Geophysical Research Letters*, 34(10), 1–8.  
641 <https://doi.org/10.1029/2006GL028999>

642 Yeager, S. G., Castruccio, F., Chang, P., Danabasoglu, G., & Maroon, E. (2021). An Outsized  
643 Role for the Labrador Sea in the Multidecadal Variability of the Atlantic Overturning  
644 Circulation. *Science Advances [PREPRINT]*, (October), 1–25.



645 Zhai, Y., Yang, J., Wan, X., & Zou, S. (2021). The Eastern Atlantic Basin Pathway for the  
646 Export of the North Atlantic Deep Waters. *Geophysical Research Letters*, *48*(24), 1–10.  
647 <https://doi.org/10.1029/2021GL095615>  
648 Zou, S., Lozier, M. S., Li, F., Abernathy, R., & Jackson, L. (2020a). Density-compensated  
649 overturning in the Labrador Sea. *Nature Geoscience*, *13*(2), 121–126.  
650 <https://doi.org/10.1038/s41561-019-0517-1>  
651 Zou, S., Bower, A., Furey, H., Susan Lozier, M., & Xu, X. (2020b). Redrawing the  
652 Iceland–Scotland Overflow Water pathways in the North Atlantic. *Nature Communications*,  
653 *11*(1). <https://doi.org/10.1038/s41467-020-15513-4>  
654